



# Is there a one-to-one correspondence between ionospheric anomalies and large earthquakes along Longmenshan faults?

L. M. He<sup>1</sup>, L. X. Wu<sup>1,2</sup>, A. De Santis<sup>3,4</sup>, S. J. Liu<sup>1</sup>, and Y. Yang<sup>1</sup>

<sup>1</sup>Institute for Geo-informatics & Digital Mine Research, College of Resources and Civil Engineering, Northeastern University, Shenyang, China

<sup>2</sup>IoT & Perception Mine Research Center, China University of Mining and Technology, Xuzhou, China

<sup>3</sup>Istituto Nazionale di Geofisica e Vulcanologia, Rome, Italy

<sup>4</sup>G. D'Annunzio University, Chieti, Italy

Correspondence to: L. X. Wu (awulixin@263.net) and L. M. He (heliming@mail.neu.edu.cn)

Received: 24 July 2013 – Revised: 20 January 2014 – Accepted: 23 January 2014 – Published: 26 February 2014

**Abstract.** On 12 May 2008, a destructive M8.0 earthquake struck Wenchuan County (31.0° N, 103.4° E) in the Longmenshan fault zone of southwestern China. Five years later, on 20 April 2013, another terrible M7.0 earthquake struck Lushan County (30.3° N, 103.0° E) in the same fault area, only 87 km away from the epicenter of the Wenchuan earthquake. In this paper, an integrated wavelet analysis methodology is proposed to detect and diagnose ionospheric total electron content (TEC) anomalies related to seismic activities. Analytic wavelet transform is used to detect ionospheric perturbations, and then cross-wavelet analysis is used to diagnose ionospheric anomalies by gaining further insights into the dynamic relationship between the anomaly variability of ionospheric TEC and geomagnetic indices for the same set of observations. The results show that a significant ionospheric disturbance occurred on 9 May 2008 above the forthcoming epicenter, 3 days prior to the Wenchuan earthquake. However, we did not observe an ionospheric anomaly over the epicenter of the Ya'an earthquake during the 1 month period before the shock. Finally, we discuss the possible interpretations of the different seismo-ionospheric effects for the two similar earthquakes.

**Keywords.** Ionosphere (ionospheric irregularities)

## 1 Introduction

Precursors of seismic activity are not only observed within the lithosphere but also within the atmosphere and ionosphere (Pulinets and Boyarchuk, 2004; Liu et al., 2000; Kuo

et al., 2011; Jin et al., 2011). This indicates that seismic activity can excite lithospheric, atmospheric and ionospheric perturbations through mutual coupling effects. In particular, the ionospheric parameters have been found to be extremely sensitive to large earthquakes, which have been reported by a number of works (Leonard and Barnes Jr., 1965; Liu et al., 2001; Pisa et al., 2011; Zhao et al., 2008; Afraimovich et al., 2010; Liu et al., 2009; Pulinets and Ouzounov, 2011; Liperovsky et al., 2005; Shvets et al., 2004; Kon et al., 2011; Le et al., 2011; Parrot, 2012; Li and Parrot, 2013). However, in most situations the subtle signals induced by large earthquakes can be easily confused with background fluctuations and short-term disturbances due to solar and geomagnetic activity. To address the background fluctuations from solar activity, we have developed a nonlinear background removal method to handle the solar radiation background in ionospheric TEC under conditions of complex solar activity (He et al., 2012).

In addition to the ionospheric variations induced by solar activity, there are significant short-term variations in the ionosphere that are induced by rapid changes in geomagnetic activity. Thus, distinguishing the ionospheric anomaly variations induced by seismic activity or geomagnetic activity is difficult, especially when there is interference from small geomagnetic storms. Processing the data and analyzing the time series to extract the characteristics of different sources, based on the ionospheric total electron content (TEC) data, is an important challenge. Current statistical methods, such as the moving interquartile range method and the moving time window method, can only examine the relative enhancement

or diminishment of the ionospheric parameters (Zhao et al., 2008; Liu et al., 2009), but is not able to provide further insights into the essential characteristics of ionospheric disturbances, such as the frequency characteristics of the disturbance signals. However, frequency domain analysis is more resolute and efficient for signal detection and diagnosis than time domain analysis under complex situations.

Wavelet transform is a modern mathematical method used for nonlinear data analysis and has been one of the most effective techniques for analyzing the nonstationary signals (Mallat, 2008). Considering the complex time-variation and nonlinear characteristics of the ionospheric disturbance signals, we propose a novel methodology, called the integrated wavelet analysis method (IWAM), for detecting and diagnosing ionospheric anomalies associated with large earthquakes, and demonstrate the capability of the method using two great earthquakes located in the Sichuan Province of China: the M8.0 Wenchuan earthquake that occurred on 12 May 2008 and the M7.0 Ya'an earthquake that occurred on 20 April 2013.

## 2 The Wenchuan and Ya'an earthquakes

As reported by the China Seismograph Network Center (CSNC), a destructive M8.0 earthquake occurred near the town of Yingxiu (31.0° N, 103.4° E; focal depth: 19 km) in Wenchuan County, Sichuan Province, China, at 14:28 LT (06:28 UTC), on 12 May 2008. The epicenter of the great Wenchuan earthquake was located in the Longmenshan fault zone, which is a group of large faults striking NE–SW, approximately 500 km long and 30–50 km wide. The crustal motion on the faults is responsible for the uplift of the mountains relative to the lowlands of the Sichuan Basin to the east. Delineating the eastern boundary of the Qinghai-Tibet Plateau, the Longmenshan fault zone forms a border between the Bayan Kola block in the plateau and the South China block in the Eurasian Plate (Chen et al., 2007).

Five years later, at 08:02 LT (00:02 UTC) on 20 April 2013, another terrible M7.0 earthquake occurred in the same fault zone, with the epicenter located in Lushan County (30.3° N, 103.0° E; focal depth: 13 km), Ya'an City, Sichuan Province, China, 87 km away from the epicenter of the Wenchuan earthquake. Besides the evident difference in the released seismic energy (according to the difference in magnitudes), the two earthquakes were similar, both being characterized by the similar focal mechanism, an almost total absence of foreshocks and extremely high aftershock activities. The processes of tectonic reconstruction in this region of the earth's crust are not frequent, but very powerful. Twelve earthquakes with magnitudes greater than M5.0 have occurred since 1900, including the 2008 Wenchuan earthquake and the 2013 Ya'an earthquake, which have been the two most powerful earthquakes during the past 112 yr.

## 3 Data sets

### 3.1 Ionospheric data

With the unprecedented temporal and spatial coverage of observations available using the global navigation satellite system (GNSS), and the hundreds of ground continuous tracking stations distributed all over the world, the ionospheric TEC data derived from GNSS observations have been extensively utilized in ionospheric studies for detecting and measuring ionospheric irregularities and anomaly variations. The global ionosphere maps (GIMs) used in this study were generated on a daily basis at the Center for Orbit Determination in Europe (CODE), using more than 200 GNSS receivers that were continuously operated by the International GNSS Service (IGS) and other institutions. The GIMs are provided with spatial resolution of 2.5° N × 5° E in latitude and longitude, with a temporal resolution of 2 h. According to previous research results, the Wenchuan and Ya'an earthquakes are likely to have caused large-scale ionospheric disturbances because they were of high magnitude and released significant seismic energy, especially the former. Furthermore, six continuously operating GNSS stations in China (BJFS (Beijing), SHAO (Shanghai), WUHN (Wuhan), KUNM (Kunming), LHAZ (Lhasa) and URUM (Urumqi)) were used to generate the CODE GIMs. Because of its accuracy and extension, CODE GIMs allow us to clearly detect large-scale anomaly variations in the ionosphere. In this study, we utilized the CODE GIMs from 13 April 2008 to 12 May 2008 and from 22 March 2013 to 20 April 2013 for the Wenchuan earthquake and the Ya'an earthquake, respectively. The TEC data right over the epicenters were interpolated from GIMs using the method recommended by IGS (Schaer et al., 1998).

### 3.2 Preprocessing of ionospheric data

The TEC data deduced from CODE GIMs show several periodic variations and background fluctuations, which are related to the diurnal and seasonal variations, the lunar tides, the solar activity cycle, irregular solar electromagnetic radiation, et cetera. To use the data for our purposes, firstly, it is necessary to remove the solar activity background from the ionospheric data. For a more detailed description of the method used, readers are referred to He et al. (2012). Then, the main variation of TEC on the short timescale is the daily cycle due to the earth's rotation. To eliminate this effect and study the anomaly variation, we use the difference of TEC (DTEC), which is calculated as follows:

$$\text{DTEC} = \text{TEC}_{\text{obs}} - \text{TEC}_{\text{ref}}, \quad (1)$$

where the  $\text{TEC}_{\text{obs}}$  are the observed TEC, and the  $\text{TEC}_{\text{ref}}$  are calculated from the previous 15 days' moving median TEC values.

### 3.3 Geomagnetic data

It is important to take into account variations in geomagnetic activity while investigating whether the ionospheric TEC perturbations are linked to the earthquake. Generally, there are significant short-term variations in the ionosphere that are induced by rapid changes of geomagnetic activity. The most pronounced short-term changes are related to geomagnetic storms. During a geomagnetic storm, energy and momentum from the magnetosphere are deposited into the upper atmosphere through enhanced high-latitude ion convection drifts and particle precipitation. The auroral oval expands and the strong precipitation of particles produces high electron densities in the lower ionospheric F and E regions. Therefore, we investigated the nonlinear relationship between a suitable geomagnetic index and the ionospheric TEC variations before the earthquakes. We used the ap index as the geomagnetic index in this study, which is obtained from the World Data Center for Geomagnetism in Kyoto (<http://swdcwww.kugi.kyoto-u.ac.jp>).

## 4 Integrated wavelet analysis method (IWAM)

In this section, we present the first combination of the analytic wavelet transform (AWT) and the cross-wavelet transform (XWT) applied to ionospheric TEC data analysis. With regards to the ionospheric disturbance signals, it is required to extract and analyze the instantaneous components of the nonstationary signal in the time–frequency domain. Referring to the prominent advantages of AWT and XWT in identifying and diagnosing the instantaneous signals, we applied AWT to detect ionospheric TEC perturbations, and XWT to diagnose whether the ionospheric TEC perturbations were actually related to the impending earthquake.

### 4.1 Detect ionospheric perturbations by AWT

In the wavelet applications, the continuous wavelet transform (CWT) can be generalized into two categories: the analytical wavelet and the real wavelet. For an analytic wavelet,  $\psi(t)$ , its Fourier transform is  $\hat{\psi}(\omega) = 0$ , when  $\omega < 0$  (Mallat, 2008). This remarkable property gives the analytic wavelet complex analysis a great ability to analyze the features of the instantaneous signal. By using the AWT over the observed period, one can simultaneously assess the frequency and temporal variability of the local ionospheric TEC anomalies. The wavelet transform of the ionospheric perturbation signal,  $f(t)$ , is expressed as

$$\begin{aligned} W(u, s) &= \frac{1}{\sqrt{s}} \int_{-\infty}^{+\infty} f(t) \psi^* \left( \frac{t-u}{s} \right) dt \\ &= W_R(u, s) + i W_I(u, s), \end{aligned} \quad (2)$$

where  $s$  and  $u$  are the dilation and translation parameters, respectively.  $W_R$  and  $W_I$  can be written as

$$\begin{cases} W_R(u, s) = \frac{1}{\sqrt{s}} \int_{-\infty}^{+\infty} f(t) \psi_R \left( \frac{t-u}{s} \right) dt \\ W_I(u, s) = -\frac{1}{\sqrt{s}} \int_{-\infty}^{+\infty} f(t) \psi_I \left( \frac{t-u}{s} \right) dt \end{cases} \quad (3)$$

The instantaneous parameters corresponding to different scales of  $s$  of a real-valued signal  $f(t)$  are as follows:

$$W_A(u, s) = \sqrt{W_R^2(u, s) + W_I^2(u, s)}, \quad (4)$$

where  $W_A(u, s)$  is the instantaneous amplitude of  $f(t)$ . We define the square of the amplitude,  $|W_A(u, s)|^2$ , as the analytic wavelet energy density spectrum, which allows us to extract the instantaneous (squared) amplitude features from the instantaneous signal. Therefore, a suitable combination, which includes the real- and imaginary parts of the complex wavelet transform coefficients, may be able to reveal more thoroughly the subtle differences in characteristics between seismo-ionospheric anomalies and other disturbances.

### 4.2 Diagnose ionospheric perturbations by XWT

The XWT is a signal analysis method, in which the wavelet transform is combined with cross-spectrum analysis in order to obtain the mutual relationship of two time series in the time–frequency domain on multi-frequency scales. Therefore, XWT can be used to analyze the relationship between the variability of the ionospheric signal and the geophysical indices around the epicenter of the earthquake. Let two time series,  $X$  and  $Y$ , have wavelet transforms,  $W^X(u, s)$  and  $W^Y(u, s)$ . The cross-wavelet transform is defined as

$$W^{XY}(u, s) = W^X(u, s) W^{Y*}(u, s), \quad (5)$$

where  $W^{Y*}(u, s)$  is the complex conjugate of  $W^Y(u, s)$ . It can further define the cross-wavelet power spectrum as  $|W^{XY}(u, s)|$ . If the two time series have a local correlation, the cross-wavelet power spectrum will show a local common high-energy region (Grinsted et al., 2004). The wavelet cross-spectra not only allow for the depiction of the common frequency features for the geophysical index and the ionospheric TEC but also highlight the temporal variations in their relationship.

### 4.3 Choosing the optimal mother wavelets

The selection criteria of a wavelet base are different for different applications. The wavelet chosen for the present study is used to extract and diagnose the anomalous features of the ionospheric TEC. Therefore, we considered the following factors to select the suitable wavelet basis:

1. *Vanishing moments.* The vanishing moment of a wavelet has an important impact on the extraction of

anomalous features. Theoretically, the greater the order of the vanishing moment, the stronger the capacity of the wavelet transform to reflect high-frequency details of the signal. However, it is observed that the higher-order derivatives induce a wider duration of sharp peaks, which affects the precision of ionospheric perturbation localization (Cao and Qiao, 2008). Therefore, the wavelets with a much higher number of vanishing moments will lead to imperfect results, which demonstrates the importance of choosing the suitable number of vanishing moments. Furthermore, the even vanishing moments are more effective than the odd vanishing moments at reflecting the instantaneous frequency of an ionospheric perturbation (Cao and Qiao, 2008).

2. *Size of support.* The support characteristics of a wavelet function represent its decay rate. The support size in different scopes corresponds to different time–frequency localization abilities. According to the Heisenberg uncertainty principle (Mallat, 2008), it is impossible to arbitrarily reduce both time and frequency localization. Therefore, to achieve accurate localization in the frequency domain of the instantaneous signal, we should select a support size as short as possible, without prejudice to the time domain analysis. Among the wavelets with equal numbers of vanishing moments, the B-spline wavelets have the shortest support.
3. *Complex or real.* A complex wavelet function will return information about both the amplitude and phase, and it is better adapted for capturing oscillatory behaviors; however, a real wavelet function returns only a single component and can be used to isolate peaks or discontinuities.
4. *Regularity.* The regularity is intimately related to the number of vanishing moments (Mallat, 2008). It is useful to reach a regular spatial-scale representation of a wavelet transform, especially in the scale aspect. After the number of vanishing moments is determined, the regularity is less important than the other requirements, such as the size of support for ionospheric perturbation identification.

Actually, it is difficult to fully meet all of the demands on factors listed above. For the AWT and the XWT, it is particularly important to consider vanishing moments and support characteristics, in both the time and frequency domains, when selecting a wavelet base. In this study, as the most appropriate choice of the mother wavelet, we considered the complex frequency B-spline wavelet `fbsp2-1-0.5` (as named in the wavelet toolbox of MATLAB; Quarteroni et al., 2010).

## 5 Implementation

The implementation of the above methods has been performed on the Wenchuan and Ya’an earthquakes as case studies. First, the analytic wavelet energy density spectrum, representing the correlation between the daughter wavelets and the local signal over a range of scales, was applied to detect and identify ionospheric TEC anomalies. Then, the XWT, providing an efficient way to examine the mutual relationship of two time series in the time–frequency domain, was applied to diagnose whether the ionospheric TEC perturbations are related to the impending earthquake.

### 5.1 Wenchuan earthquake

The Wenchuan earthquake occurred during the period of extremely low solar activity between the 23rd and the 24th solar cycle. Over the duration of the studied period, the solar activity was nearly unchanged. Thus, the ionospheric parameter variation caused by irregular solar electromagnetic radiation is very small, and there is no need to remove the solar activity background from the ionospheric data in conditions of quiet solar activity. Figure 1 shows the DTEC time series directly over the epicenter of the Wenchuan earthquake, the analytic wavelet energy density spectrum of the DTEC and the 3-D coefficient plots of the analytic wavelet energy density spectrum. As shown in Fig. 1b, c, the energy density spectrum of the ionospheric anomaly variations contained many significant enhancements before the shock. The enhancements can be classified into two types: type I and type II. Both types of enhancements are over small scales, namely the fine scales or the high-frequency band. However, the enhancements of type I are larger than the enhancements of type II. The anomalies that appear above the Wenchuan earthquake epicenter (Table 1) show that the two type I anomalies significantly reduced at approximately 08:00 UTC on 29 April 2008 (13 days before the earthquake) and enhanced at approximately 10:00 UTC on 9 May 2008 (3 days before the earthquake). The three type II anomalies reduced at 08:00 UTC on 24 April (18 days before the earthquake), enhanced at approximately 04:00 UTC on 21 April 2008 (21 days before the earthquake) and enhanced at approximately 08:00 UTC on 18 April 2008 (24 days before the earthquake).

Are these disturbances associated with the M8.0 Wenchuan earthquake? As mentioned above, geomagnetic activity can also cause ionospheric TEC variations. Geomagnetic activity variations not only cause global changes but also cause well-pronounced local perturbations of the ionospheric parameters that can mask the processes occurring before an earthquake (Rishbeth, 2006; Dautermann et al., 2007; Afraimovich and Astafyeva, 2008). Because of the easily confused effects caused by geomagnetic activity in the ionosphere, the geomagnetic conditions should be taken into account. Therefore, it is necessary to analyze the geomagnetic index as an indicator of geomagnetic disturbance. In

**Table 1.** Ionospheric perturbations before the Wenchuan earthquake detected by AWT and DTEC from 13 April to 12 May 2008. The + and – signs stand for the positive and negative perturbations detected by DTEC, respectively.

Type of anomalies	Date	UTC time	Local time	±	Before days
I	29 Apr 2008	08:00	15:00	–	13
	9 May 2008	10:00	17:00	+	3
II	18 Apr 2008	08:00	15:00	+	24
	21 Apr 2008	04:00	11:00	+	21
	24 Apr 2008	08:00	15:00	–	18

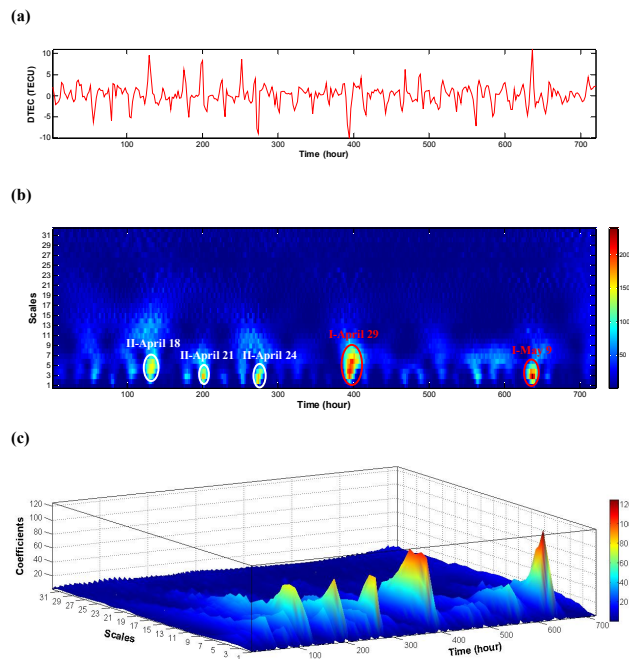


**Fig. 1.** (a) The DTEC time series right over the epicenter ( $31.0^{\circ}$  N,  $103.4^{\circ}$  E) of the Wenchuan earthquake from 13 April to 12 May, 2008. (b) The analytic wavelet energy density spectrum of DTEC using fbsp2-1-0.5 wavelet. The thick red ellipse designates the “I” style significant enhancement. The thick white ellipse designates the “II” style significant enhancement. (c) The 3-D coefficient plots of the analytic wavelet energy density spectrum.

this study, the geomagnetic index,  $a_p$ , was used to assess the specific link between the geomagnetic activity and the ionospheric TEC perturbations occurring before the earthquake.

Figure 2 shows the cross-wavelet spectrum for the DTEC and  $a_p$ . This plot shows that several common high-energy regions exist within the two time series. The first and the second common high-energy regions are marked by white rectangles, corresponding to the long time effect for the periods 12–18 April 2008 and 20–26 April 2008, respectively. The reason is that the ionosphere can be enhanced or decreased during the geomagnetic activity period for several days before and after a geomagnetic storm (Liu et al., 2008a, b; Zhao et al., 2009; Mikhailov and Perrone, 2009). In addition, many

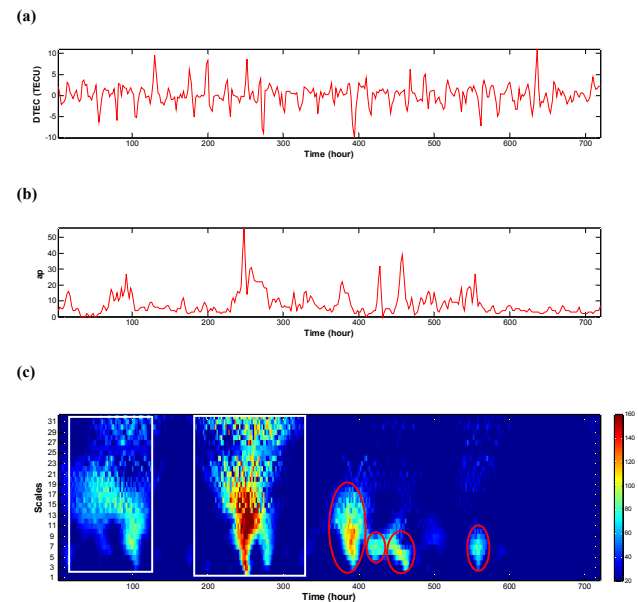


**Fig. 2.** (a) The DTEC time series right over the epicenter ( $31.0^{\circ}$  N,  $103.4^{\circ}$  E) of the Wenchuan earthquake from 13 April to 12 May, 2008. (b) The variations of the  $a_p$  geomagnetic index from 13 April to 12 May, 2008. (c) The cross-wavelet spectrum for DTEC and  $a_p$  using fbsp2-1-0.5 wavelet.

high-energy regions containing short time effects (marked by red ellipses) also emerged, corresponding to the dates 29 and 30 April and 1 and 6 May 2008, respectively. The relationship between the ionospheric anomaly variations and the geomagnetic activity has been summarized in Table 2. It is easy to identify the disturbances on 29, 24, 21, and 18 April 2008 detected by the AWT; these were most likely linked to geomagnetic activity. Three high-energy regions on 30 April, 1 May and 6 May 2008 detected by the XWT show that geomagnetic activity had less effect on the ionosphere in the epicenter region. Hence, we deduced that these slight disturbances in the DTEC directly over the epicenter were not detected by the AWT.

To check if the TEC disturbances of 9 May 2008 specifically appear in the earthquake region, we have processed several points interpolated from GIMs far from the earthquake preparation zone, but at the same latitude of the Wenchuan

**Table 2.** The relationship between the ionospheric anomaly variations and the geomagnetic activity before the Wenchuan earthquake from 13 April 2008 to 12 May 2008.

Common high-energy region detected by XWT	Disturbances detected by AWT	Affected by geomagnetic activities
12–18/4/2008	18/4/2008	Y
20–26/4/2008	21/4/2008	Y
	24/4/2008	Y
29/4/2008	29/4/2008	Y
30/4/2008	–	Y
1/5/2008	–	Y
6/5/2008	–	Y
–	9/5/2008	N

epicenter (Fig. 3). It can be seen that the TEC disturbances that occurred on 9 May 2008 right over the epicenter did not appear in other locations where no earthquake happened. Furthermore, we have processed the data for 2007 and 2006 within the same location of the Wenchuan epicenter and time period of 2008 using the same method, respectively. We did not find anomaly disturbance except for some disturbances related to some geomagnetic activity.

To further investigate the spatial characteristics of ionospheric anomalies on 9 May 2008, we define a seismo-ionospheric anomaly index as the maximum enhancement among the fine-scale (1 ~ 10) variations in the complex analytic wavelet energy density spectrum at each time and grid point. Figure 4 shows the evolution of two-dimensional maps for the seismo-ionospheric anomaly index during the time frame 00:00–16:00 UT on 9 May 2008. It shows that the enhancement of TEC disturbances started at 04:00 UT (12:00 LT) with maximum amplitude appearing southeast of the epicenter. After 6 h, the disturbances were expanded and amplified, reaching to its maximum value at 10:00 UT. Then, the TEC disturbances disappeared around 16:00 UT in the whole region. The observation indicated that the abnormal disturbances of ionospheric TEC was localized within an area between longitudes 90–130° E and latitudes 15–35° N, and slight disturbances also appeared around its southern conjugate region.

Overall, considering the geophysical conditions during the observation period and the capability of the algorithm used, the anomaly ionospheric TEC variations that appeared on 9 May 2008 should be associated with the impending Wenchuan earthquake.

## 5.2 Ya'an earthquake

The Ya'an earthquake occurred during the period of high solar activity in the 24th solar cycle. There is a strong nonlinear background in the TEC data, caused by irregular solar electromagnetic radiation during the study period (Fig. 5). It is necessary to remove the solar activity background in the ionospheric data to avoid possible introducing error in the

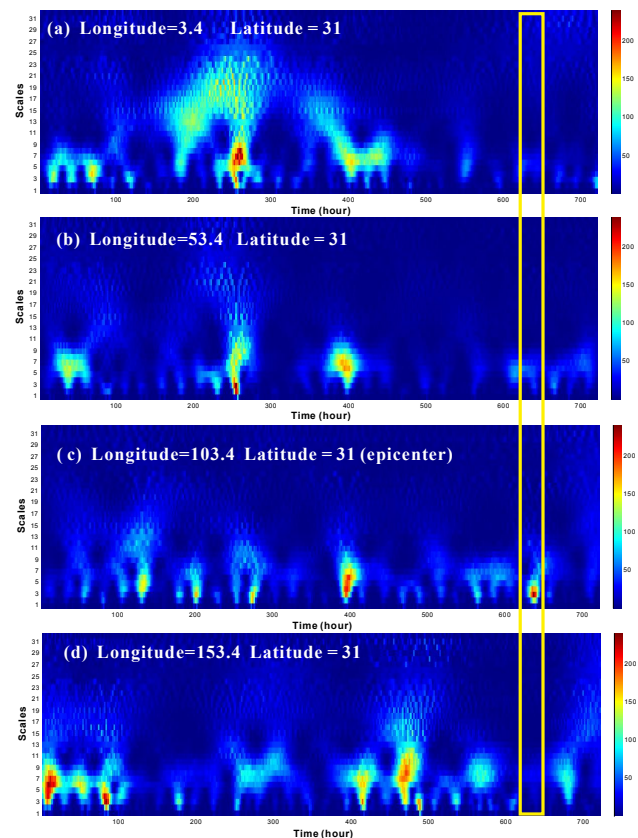


**Fig. 3.** The analytic wavelet energy density spectrum of DTEC time series from 13 April to 12 May 2008 right over the locations: (a) latitude = 31° N, longitude = 3.4° E; (b) latitude = 31° N, longitude = 53.4° E; (c) latitude = 31° N, longitude = 103.4° E (epicenter); (d) latitude = 31° N, longitude = 153.4° E.

DTEC time series. Figure 5 shows that there is a high correlation between the extracted background and the solar activity index F10.7. Thus, the nonlinear background can be eliminated using the method presented in He et al. (2012).

Figure 6 shows the DTEC time series directly over the epicenter of the Ya'an earthquake, the analytic wavelet energy density spectrum of the DTEC and the 3-D coefficient plots

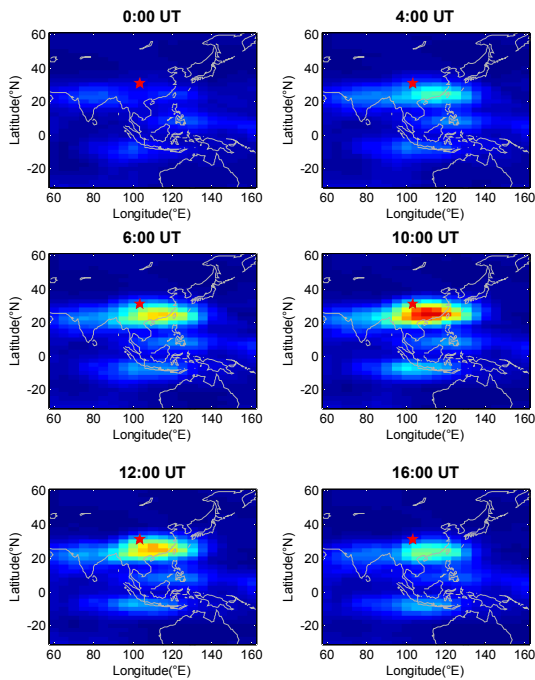


**Fig. 4.** Two-dimensional maps for small scales of analytic wavelet energy density spectrum on 9 May 2008 from 00:00 to 16:00 UT. The red star represents the epicenter.

of the analytic wavelet energy density spectrum. It can be seen that only one positive significant enhancement appeared at 08:00 UTC (16:00 LT) on 24 March 2013, 27 days before the shock.

To discern whether the ionospheric disturbance detected by the AWT is linked to geomagnetic activity, we performed the XWT for the DTEC and ap time series before the earthquake. Figure 7 shows the cross-wavelet spectrum for the DTEC and ap. It reveals that there are three common high-energy regions (marked by white rectangles) existing within the two time series. The first common high-energy region corresponds to 24 March 2013. Therefore, this enhancement was more likely associated with the geomagnetic storm effects. Considering the solar and geomagnetic activity conditions, we did not find an ionospheric anomaly directly over the epicenter of the Ya’an earthquake during the 1 month period before the shock.

Furthermore, according to the previous studies (Pulinets and Boyarchuk, 2004; Zhao et al., 2008), the TEC anomalies before large earthquakes always appeared in the southeast or southwest of the epicenter for earthquakes located in the middle latitude of the Northern Hemisphere. Therefore, we have checked several points in the southeast and southwest of the Ya’an earthquake epicenter interpolated from CODE GIMs, and all the results show also that no significant TEC disturbance appeared during the studied period over these points, which were located in equatorial latitudes, except for some perturbations associated with the geomagnetic storms.

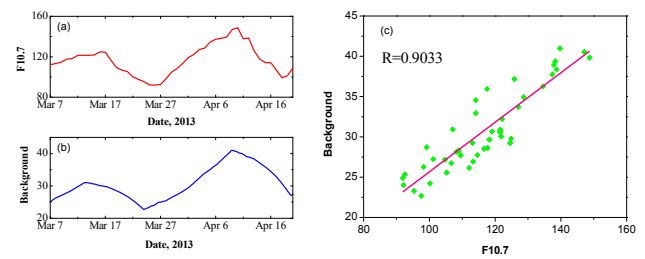


**Fig. 5.** (a) Solar activity index F10.7 time series. (b) Decomposed TEC background time series. (c) The Pearson correlation between the background and F10.7.

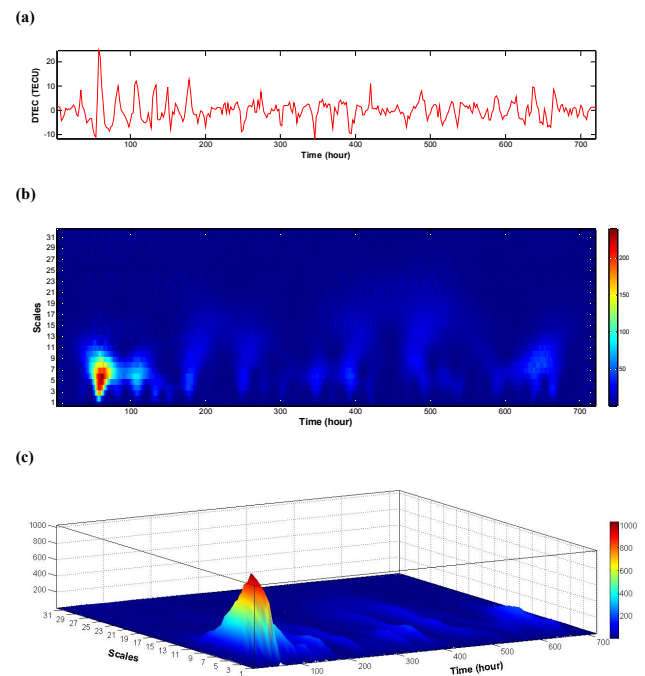


**Fig. 6.** (a) The DTEC time series right over the epicenter (30.3° N, 103.0° E) of the Ya’an earthquake from 22 March 2013 to 20 April 2013. (b) The analytic wavelet energy density spectrum of DTEC using fbsp2-1-0.5 wavelet. (c) The 3-D coefficient plots of the analytic wavelet energy density spectrum.

## 6 Discussion and conclusion

Possible ionospheric TEC anomalies preceding two large earthquakes, the M8.0 Wenchuan earthquake and the M7.0 Lushan earthquake, along the Longmenshan fault zone, are detected and diagnosed by IWAM. Enhancement of ionospheric TEC anomalies occurred 3 days before the Wenchuan earthquake, right over the epicenter, which is consistent with the TEC time-varying analysis results obtained by Zhao et al. (2008). However, no expected TEC anomaly over the epicenter of the Ya’an earthquake was detected. It is noteworthy that the solar activity before and after Ya’an earthquake had rapid and intensive variations, whereas the solar

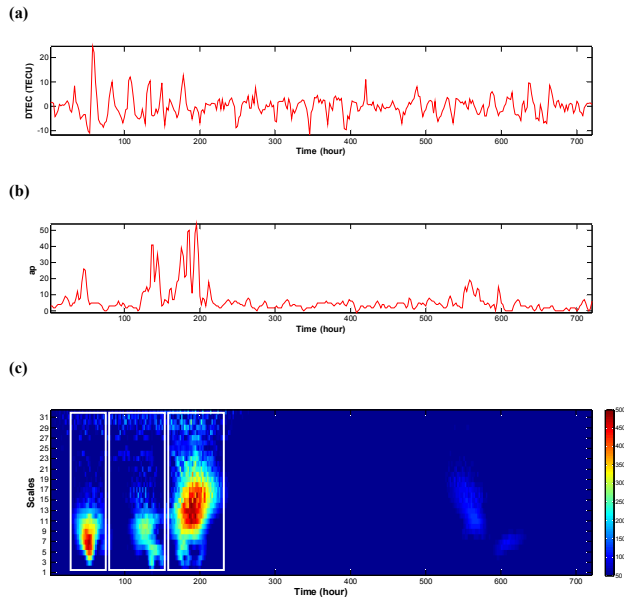


**Fig. 7.** (a) The DTEC time series right over the epicenter ( $30.3^{\circ}$  N,  $103.0^{\circ}$  E) of the Ya'an earthquake from 22 March 2013 to 20 April 2013. (b) The variations of the ap geomagnetic index from 22 March 2013 to 20 April 2013. (c) The cross-wavelet spectrum for DTEC and ap using fbsp2-1-0.5 wavelet.

activity was extremely low before and after Wenchuan earthquake. We can ignore the influence of solar electromagnetic radiation when analyzing the ionospheric anomalies before the Wenchuan earthquake due to the fact that solar activity was nearly unchanged. However, the situation was completely different for the Ya'an earthquake: if we don't consider the strong effect from irregular solar electromagnetic radiation, the ionospheric variations caused by solar activity would be misjudged as ionospheric anomalies caused by the earthquake.

In general, during the processes developing before a large earthquake, the regional tectonic stresses change sequentially before the shock. Meanwhile, a series of physical and chemical variations occur within the lithosphere. How can it reach ionospheric height and make ionospheric TEC unusual? Pulnits and Ouzounov (2011) suggested that the increasing radon emanation carried by many gases in seismically active regions can ionize the near air with particles produced by radon decay, and can generate a considerable vertical electric field between the ground and the ionosphere. The strong vertical electric field could modify ionospheric dynamics and electron density distribution before the onset of a large earthquake. The simulation results from a quasi-electrostatic model of atmosphere–thermosphere–ionosphere coupling concluded that a vertical electric field of approximately  $1 \text{ kV m}^{-1}$  at the earth's surface could generate a horizontal electric field of approximately  $1 \text{ mV m}^{-1}$  in the ionosphere (Pulnits et al., 2000; Pulnits and Boyarchuk, 2004).

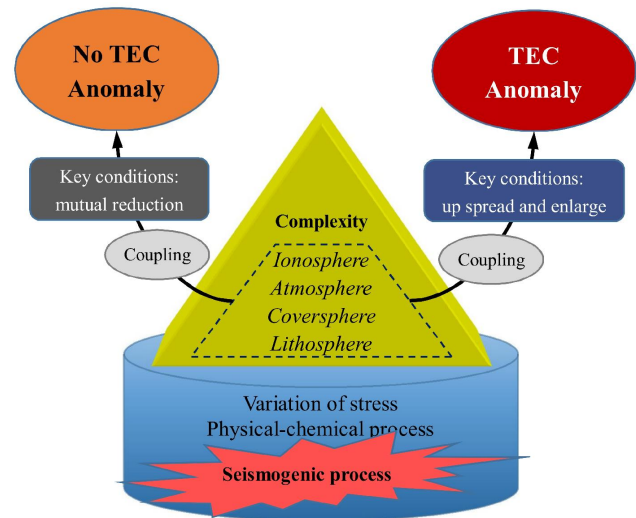


**Fig. 8.** Schematic plot for interpreting whether the TEC anomalies are generated by earthquakes.

Rock-loading laboratory experiments conducted by Freund (2000) showed that mobile positive holes (p-holes) could be activated by microfractures before rock fracturing. The spreading out of these p-holes can further produce currents and electromagnetic effects on the earth's surface, and the upward expansion of ionized air can change the electron density in the ionosphere (Freund, 2011). Meanwhile, the diffusion and outflow of these p-holes can also generate high electric fields at the earth's surface, which can penetrate into the ionosphere and change the ionospheric TEC distribution in sequence.

Recently, the simulation results from a coupling model for the stressed rock–earth surface charges–atmosphere–ionosphere system developed by Kuo et al. (2011), have shown that a current density  $J_{\text{rock}} = 0.2\text{--}10 \mu\text{A m}^{-2}$  in an earthquake fault zone could cause daytime TEC variations of 2–25%. Other simulation results show that a current density  $J_{\text{rock}} = 0.01\text{--}1 \mu\text{A m}^{-2}$  can lead to nighttime TEC variations of 1–30%, as well as the formation of a nighttime plasma bubble (equatorial spread F) extending over the whole magnetic flux tube containing the earthquake epicenter.

The absence of seismo-ionospheric anomaly before the 2013 Ya'an mainshock could be due to a possible reduced energy of earthquake preparation (seen its lower magnitude than that of 2008 Wenchuan earthquake). Besides, the absence of the proper coversphere conditions (Wu et al., 2012), which allow the transfer of the lithospheric energy to the ionosphere, could be another cause that prevents the lithosphere–ionosphere coupling. It is clear that the initial variations in the lithosphere caused by a seismogenic process, especially several days preceding the shock, should be considerable and that these variations can propagate outward and upward (Fig. 8). In fact, this indicates that there are at

least two basic conditions that result in seismo-ionospheric anomalies: (1) the stress variations and physical–chemical processes preceding a strong earthquake should have generated enough electromagnetic signals and (2) the coversphere of seismogenic zone possesses the conditions, such as soil electrical field and ionized pore gas simulated by tectonic stress, required to propagate the electromagnetic effects outward and upward, possibly reaching to ionospheric heights. The key point is that the local coversphere should have the ability to enlarge and expand the upward electromagnetic signals, and create unusual ionospheric TEC anomalies. If the coversphere declines, reduces, or contracts the outward electromagnetic signals, the ionospheric electron density anomalies cannot be observed.

Although the generation mechanisms of electromagnetic signals from seismogenic zone are not well understood, the presented novel methodology for analyzing the time–frequency characteristics of ionospheric anomalies is capable of detecting and diagnosing the ionospheric variations possibly associated with earthquakes in unquiet solar-terrestrial environments, especially for earthquakes and geomagnetic storms.

*Acknowledgements.* This research was supported by the National Important Basic Research Project (Grant No. 2011CB707102), the National Natural Science Foundation of China (Grant No. 41104104), and the Fundamental Research Funds for the Central Universities (Grant No. N120801001). We thank all the anonymous referees for their constructive and thorough reviews. The authors acknowledge the International GNSS Service (IGS) and the Center for Orbit Determination in Europe (CODE) for providing the GPS TEC data. The F10.7 and ap indices were downloaded from the NGDC database.

Topical Editor K. Hosokawa thanks three anonymous referees for their help in evaluating this paper.

## References

- Afraimovich, E. and Astafyeva, E.: TEC anomalies – Local TEC changes prior to earthquakes or TEC response to solar and geomagnetic activity changes?, *Earth Planets Space*, 60, 961–966, 2008.
- Afraimovich, E., Ding, F., and Kiryushkin, V.: TEC response to the 2008 Wenchuan Earthquake in comparison with other strong earthquakes, *Int. J. Remote Sens.*, 31, 3601–3613, doi:10.1080/01431161003727747, 2010.
- Cao, M. and Qiao, P.: Integrated wavelet transform and its application to vibration mode shapes for the damage detection of beam-type structures, *Smart Mater. Struct.*, 17, 055014, doi:10.1088/0964-1726/17/5/055014, 2008.
- Chen, G. G., Ji, F. J., Zhou, R. J., Xu, J., Zhou, B. G., Li, X. G., and Ye, Y. Q.: Primary research of activity segmentation of Longmenshan fault zone since Late-Quaternary, *Seismol. Geol.*, 29, 657–673, 2007 (in Chinese).
- Dautermann, T., Calais, E., Haase, J., and Garrison, J.: Investigation of ionospheric electron content variations before earthquakes in southern California, 2003–2004, *J. Geophys. Res.*, 112, B02106, doi:10.1029/2006JB004447, 2007.
- Freund, F.: Time-resolved study of charge generation and propagation in igneous rocks, *J. Geophys. Res.*, 105, 11001, doi:10.1029/1999JB900423, 2000.
- Freund, F.: Pre-earthquake signals: Underlying physical processes, *J. Asian Earth Sci.*, 41, 383–400, doi:10.1016/j.jseaes.2010.03.009, 2011.
- Grinsted, A., Moore, J., and Jevrejeva, S.: Application of the cross wavelet transform and wavelet coherence to geophysical time series, *Nonlinear Proc. Geoph.*, 11, 561–566, 2004.
- He, L., Wu, L., Pulnits, S., Liu, S., and Yang, F.: A nonlinear background removal method for seismo-ionospheric anomaly analysis under a complex solar activity scenario: A case study of the M9.0 Tohoku earthquake, *Adv. Space Res.*, 50, 211–220, doi:10.1016/j.asr.2012.04.001, 2012.
- Jin, S., Han, L., and Cho, J.: Lower atmospheric anomalies following the 2008 Wenchuan Earthquake observed by GPS measurements, *J. Atmos. Sol.-Terr. Phys.*, 73, 810–814, doi:10.1016/j.jastp.2011.01.023, 2011.
- Kon, S., Nishihashi, M., and Hattori, K.: Ionospheric anomalies possibly associated with  $M \geq 6.0$  earthquakes in the Japan area during 1998–2010: Case studies and statistical study, *J. Asian Earth Sci.*, 41, 410–420, doi:10.1016/j.jseaes.2010.10.005, 2011.
- Kuo, C., Huba, J., Joyce, G., and Lee, L.: Ionosphere plasma bubbles and density variations induced by pre-earthquake rock currents and associated surface charges, *J. Geophys. Res.*, 116, A10317, doi:10.1029/2011JA016628, 2011.
- Le, H., Liu, J., and Liu, L.: A statistical analysis of ionospheric anomalies before 736 M6.0+ earthquakes during 2002–2010, *J. Geophys. Res.*, 116, A02303, doi:10.1029/2010JA015781, 2011.
- Leonard, R. and Barnes Jr., R.: Observations of ionospheric disturbances following the Alaska earthquake, *J. Geophys. Res.*, 70, 1250–1253, doi:10.1029/JZ070i005p01250, 1965.
- Li, M. and Parrot, M.: Statistical analysis of an ionospheric parameter as a base for earthquake prediction, *J. Geophys. Res.*, 118, 3731–3739, doi:10.1002/jgra.50313, 2013.
- Liperovsky, V. A., Meister, C.-V., Liperovskaya, E. V., Vasil'eva, N. E., and Alimov, O.: On spread-Es effects in the ionosphere before earthquakes, *Nat. Hazards Earth Syst. Sci.*, 5, 59–62, doi:10.5194/nhess-5-59-2005, 2005.
- Liu, J., Chen, Y., Pulnits, S., Tsai, Y., and Chuo, Y.: Seismo-ionospheric signatures prior to  $M \geq 6.0$  Taiwan earthquakes, *Geophys. Res. Lett.*, 27, 3113–3116, doi:10.1029/2000GL011395, 2000.
- Liu, J., Chen, Y., Chuo, Y., and Tsai, H.: Variations of ionospheric total electron content during the Chi-Chi Earthquake, *Geophys. Res. Lett.*, 28, 1383–1386, doi:10.1029/2000GL012511, 2001.
- Liu, J., Chen, Y., Chen, C., Liu, C., Chen, C., Nishihashi, M., Li, J., Xia, Y., Oyama, K., and Hattori, K.: Seismoionospheric GPS total electron content anomalies observed before the 12 May 2008 Mw7.9 Wenchuan earthquake, *J. Geophys. Res.*, 114, A04320, doi:10.1029/2008JA013698, 2009.
- Liu, L., Wan, W., Zhang, M., Zhao, B., and Ning, B.: Prestorm enhancements in  $NmF2$  and total electron content at low latitudes, *J. Geophys. Res.*, 113, A02311, doi:10.1029/2007JA012832, 2008a.
- Liu, Libo, Wan, Weixing, Zhang, Man-Lian, and Zhao, Biqiang: Case study on total electron content enhancements at low lati-

- tudes during low geomagnetic activities before the storms, *Ann. Geophys.*, 26, 893–903, doi:10.5194/angeo-26-893-2008, 2008b.
- Mallat, S.: *A Wavelet Tour of Signal Processing*, Third Edition: The Sparse Way, Academic Press, 2008.
- Mikhailov, A. V. and Perrone, L.: Pre-storm  $NmF2$  enhancements at middle latitudes: delusion or reality?, *Ann. Geophys.*, 27, 1321–1330, doi:10.5194/angeo-27-1321-2009, 2009.
- Parrot, M.: Statistical analysis of automatically detected ion density variations recorded by DEMETER and their relation to seismic activity, *Ann. Geophys. Italy*, 55, 149–155, doi:10.4401/ag-5270, 2012.
- Pisa, D., Parrot, M., and Santolík, O.: Ionospheric density variations recorded before the 2010 Mw 8.8 earthquake in Chile, *J. Geophys. Res.*, 116, A08309, doi:10.1029/2011ja016611, 2011.
- Pulinets, S. and Boyarchuk, K.: *Ionospheric precursors of earthquakes*, Springer Verlag, Berlin, 2004.
- Pulinets, S. and Ouzounov, D.: Lithosphere-Atmosphere-Ionosphere Coupling (LAIC) model – An unified concept for earthquake precursors validation, *J. Asian Earth Sci.*, 41, 371–382, doi:10.1016/j.jseaes.2010.03.005, 2011.
- Pulinets, S., Boyarchuk, K., Hegai, V., Kim, V., and Lomonosov, A.: Quasielectrostatic model of atmosphere-thermosphere-ionosphere coupling, *Adv. Space Res.*, 26, 1209–1218, doi:10.1016/S0273-1177(99)01223-5, 2000.
- Quarteroni, A., Gervasio, P., and Saleri, F.: *Scientific computing with MATLAB and Octave*, Springer, 2010.
- Rishbeth, H.: Ionoquakes: Earthquake precursors in the ionosphere?, *Eos. T. Am. Geophys. Un.*, 87, p. 316, doi:10.1029/2006EO320008, 2006.
- Schaer, S., Gurtner, W., and Feltens, J.: IONEX: The ionosphere map exchange format version 1, *Proceedings of the IGS AC Workshop*, Darmstadt, Germany, 1998.
- Shvets, A. V., Hayakawa, M., and Maekawa, S.: Results of subionospheric radio LF monitoring prior to the Tokachi (M=8, Hokkaido, 25 September 2003) earthquake, *Nat. Hazards Earth Syst. Sci.*, 4, 647–653, doi:10.5194/nhess-4-647-2004, 2004.
- Wu, L., Qin, K., and Liu, S.: GEOS-Based Thermal Parameters Analysis for Earthquake Anomaly Recognition, *Proc. IEEE*, 100, 2891–2907, doi:10.1109/JPROC.2012.2184789, 2012.
- Zhao, B., Wang, M., Yu, T., Wan, W., Lei, J., Liu, L., and Ning, B.: Is an unusual large enhancement of ionospheric electron density linked with the 2008 great Wenchuan earthquake?, *J. Geophys. Res.*, 113, A11304, doi:10.1029/2008JA013613, 2008.
- Zhao, B., Wan, W., Liu, L., Igarashi, K., Yumoto, K., and Ning, B.: Ionospheric response to the geomagnetic storm on 13–17 April 2006 in the West Pacific region, *J. Atmos. Sol.-Terr. Phys.*, 71, 88–100, doi:10.1016/j.jastp.2008.09.029, 2009.